

Nonlocal two-photon interference of energy-time entangled photon pairs generated in Doppler-broadened ladder-type ^{87}Rb atoms

Gyu-Hyeok Lee ,* Yong Sup Ihn, Ahreum Lee , U-Shin Kim, and Yoon-Ho Kim [†]

Department of Physics, Pohang University of Science and Technology (POSTECH), Pohang 37673, Korea



(Received 22 July 2019; published 8 November 2019)

We experimentally demonstrate nonlocal two-photon interference of energy-time entangled photon pairs via spontaneous four-wave mixing (SFWM) process in Doppler-broadened ladder-type ^{87}Rb atoms. The Doppler-broadened ladder-type atomic system offers collective two-photon coherence which results in strong temporal correlation between the entangled photons. The spacelike separated photon pairs clearly show nonlocal two-photon interference with high visibility of $97.1 \pm 2.5\%$, which violates the Bell-CHSH (Clauser-Horne-Shimony-Holt) inequality by 10.5 standard deviations, in which the travel time of a single-photon towards the interferometer is much longer than the coincidence window. Our work will provide an atom-based entangled photon source which is applicable for long distance atom-memory-based quantum communication.

DOI: [10.1103/PhysRevA.100.053817](https://doi.org/10.1103/PhysRevA.100.053817)

I. INTRODUCTION

It is now well established that entangled quantum systems, contradictory to the local hidden variable theories, may provide nonlocal correlation between remote measurement outcomes [1]. To date, experimental research on nonlocal quantum correlation has usually been carried out by utilizing entangled photons from the spontaneous parametric down-conversion (SPDC) process in a nonlinear crystal. The SPDC photons, however, have a rather broad spectral bandwidth, resulting in a typical coherence time on the order of a few hundreds of femtoseconds [2,3]. Since typical atomic quantum memory can store and retrieve photons with a coherence time in the timescale of μs [4–8], the SPDC photons in general do not efficiently interact with the atomic quantum memory system. To this end, the cavity-assisted SPDC process has been engineered to provide narrow-band photon pairs [9,10].

On the other hand, spontaneous four-wave mixing (SFWM) in an atomic system offers a natural narrow-band source of entangled photon pairs, and the SFWM photons may efficiently interact with the atomic quantum memory system [11–14]. A cold atom system has been used as a source of the SFWM photons. The cold atom system, however, is rather complicated, and the photon pair generation rate in the cold atom system is much lower than the SPDC process in a nonlinear crystal. To overcome the limits of the cold atom system, photon pair generation in a hot atom system has been researched [15,16]. The hot atom system is rather simple, and the photon pair generation rate is higher than in the cold atom system. Especially, cascade emission from the hot atom system with ladder-type energy level shows a high photon pair generation rate compatible with the SPDC process [17].

The SFWM photons are naturally energy-time entangled. A Franson interferometer has been used to test energy-time entanglement of the entangled photons [18–25]. In the

Franson interferometer, any single-photon interference is totally eliminated because the path-length difference between the long path and short path is much longer than the coherence length of the input photons [26,27]. Therefore, interference observed in the coincidence rate is genuine two-photon interference. Time-bin encoded quantum key distribution experiments also have been explored by using a Franson interferometer [28–31]. Since two-photon interference originates from nonlocal temporal correlation between the entangled photons, spacelike separated photon pairs can exhibit two-photon interference in which the single-photon travel time towards the interferometer is considerably longer than the coincidence window [32]. Here, we report nonlocal two-photon interference of the energy-time entangled photon pairs via the SFWM process in Doppler-broadened ladder-type ^{87}Rb atoms.

II. ENERGY-TIME ENTANGLED PHOTON PAIR GENERATION

The experimental setup for the SFWM process is shown in Fig. 1(a). The Rb cell is heated to 70°C and shielded by the three layers of μ metal to shield the earth's magnetic field. The horizontally polarized pump beam and the vertically polarized coupling beam counterpropagate inside the Rb cell. The signal and idler photons are generated via the SFWM process. We set the phase matching angle as 1.43° . The SFWM photon pairs and the laser beams are spatially separated, but the laser beams are scattered from the Rb cell so that they contribute to noise. To filter out the noise by means of polarization optics, we used polarizing beam splitters (PBSs) and Glan-Thompson polarizers.

Figure 1(b) presents the schematic ladder-type energy level of the ^{87}Rb atom used for generating the energy-time entangled photon pairs. The pump laser is blue-detuned by 1 GHz from the $|5S_{1/2}, F=2\rangle \rightarrow |5P_{3/2}, F'=3\rangle$ transition. The detuning for the pump laser is for suppressing spontaneous emission from the intermediate state $|5P_{3/2}, F'=3\rangle$. The coupling laser is red-detuned by 1 GHz from the

*gyuhyeoklee@gmail.com

[†]yoonho72@gmail.com

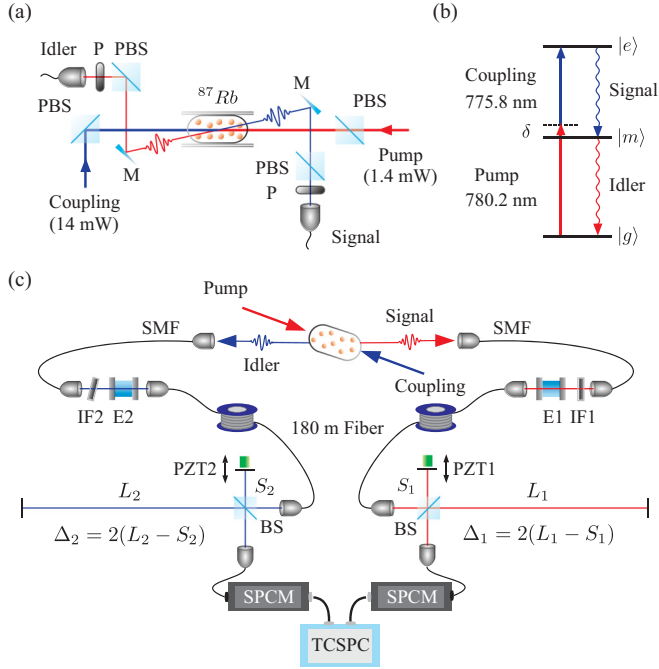


FIG. 1. (a) Schematic of spontaneous four-wave mixing in the experiment. Horizontally polarized pump field and vertically polarized coupling field counterpropagate inside the Rb cell. Generated signal and idler photons are filtered by means of PBSs and polarizers (P) and coupled into a single-mode fiber. (P: Glan-Thompson polarizer; M: Mirror.) (b) The ladder-type energy level of ^{87}Rb . The energy-time entangled photon pairs, the signal and idler photons, are generated by cascade emission in the ^{87}Rb vapor. ($\delta = 1$ GHz, $|g\rangle = |5S_{1/2}, F = 2\rangle$, $|m\rangle = |5P_{3/2}, F' = 3\rangle$, $|e\rangle = |5D_{5/2}, F'' = 4\rangle$). (c) Schematic of nonlocal two-photon interference experiment. Each single photon is filtered by the interference filter (IF) and the solid fused-silica etalon filter (E). The SFWM photon pair source and the interferometer are separated by a 180 m fiber, so two-photon interference is a nonlocal event. The path-length difference between the long and short paths in each unbalanced Michelson-Morley interferometer is 1.5 m. (SMF: Single-mode fiber; IF: Interference filter; E: Solid fused-silica etalon filter; BS: Beam splitter; PZT: Piezo transducer; SPCM: Single-photon-counting module; TCSPC: Time-correlated single-photon counting module.)

$|5P_{3/2}, F' = 3\rangle \rightarrow |5D_{5/2}, F'' = 4\rangle$ transition. This configuration makes the collective two-photon coherence effect of the Doppler-broadened ladder-type atomic ensemble.

The spectral filters were used for filtering the residual pump and coupling beam as shown in Fig. 1(c). Each interference filter's full width at half maximum (FWHM) bandwidth is 1 nm. The interference filters for idler photons (IF1) and signal photons (IF2) have transmission peaks of 92% and 95%, respectively. The etalon filters have 1 GHz FWHM bandwidth. The etalon filters for idler photons (E1) and signal photons (E2) have transmission peaks of 93% and 91%, respectively.

The direction of the coupling and pump noise scattered from the Rb cell can be changed by tilting the Rb cell, so we can maximize the signal-to-noise ratio (SNR) of the single counts of the single photons. The SNR of the signal photons is $96\,000\text{ Hz}/7000\text{ Hz} \cong 13.7$ and that of the idler photons

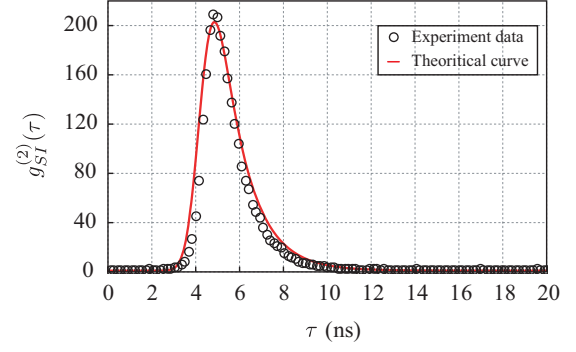


FIG. 2. Normalized cross-correlation function for the signal and idler photons. Total integration time of coincidence events histogram is 30 s. The red curve is a theoretical result of the normalized cross-correlation function for the photon pairs generated in the Doppler-broadened atoms, which is calculated by using Eq. (1).

is $45\,600\text{ Hz}/3400\text{ Hz} \cong 13.4$. The coincidence counts of the signal and idler photons is 2300 Hz with the coincidence window of 6.8 ns.

The normalized cross-correlation function $g_{SI}^{(2)}(\tau)$ for the signal and idler photons is shown in Fig. 2. The output signal from the signal (idler) photon detection event is used as the start (stop) for the time-correlated single-photon counting module. The coincidence event between the signal and idler photons is obtained by the histogram for a given time delay between the start and stop signals. The cross-correlation function $G_{SI}^{(2)}(\tau)$ for photon pairs generated in Doppler-broadened atoms is defined as

$$G_{SI}^{(2)}(\tau) = \left| \int \Psi_v(\tau) f(v) dv \right|^2, \quad (1)$$

where $\Psi_v(\tau)$ is the wave function of a photon pair generated in Doppler-broadened ladder-type ^{87}Rb atoms via the SFWM process and $f(v)$ is the Maxwell-Boltzmann velocity distribution in one dimension [16,17]. To show genuine temporal correlation between the signal and idler photons, $G_{SI}^{(2)}(\tau)$ is normalized to $g_{SI}^{(2)}(\tau)$. The normalized cross-correlation function $g_{SI}^{(2)}(\tau)$ is shown as the red curve in Fig. 2, and it is well matched with the time-correlated single-photon counting measurements. The maximum value of $g_{SI}^{(2)}(\tau)$ is 203, which shows strong temporal correlation between the signal and idler photons.

When two-photon resonance condition is satisfied, strong temporal correlation is generated between the entangled photons. The two-photon resonance condition for the Doppler-broadened Rb ensemble is defined as

$$\delta_p + k_p v + \delta_c + k_c v = 0, \quad (2)$$

where δ_p (δ_c) is the detuning of the pump (coupling) laser, k_p (k_c) is the wave vector of the pump (coupling) laser, and v represents the velocity of a Rb atom. The pump laser and the coupling laser, which have similar wavelength, counterpropagating the Doppler-broadened Rb ensemble have almost same Doppler-frequency shift, but the signs of the Doppler-frequency shifting are opposite (i.e., $k_p v + k_c v \cong 0$). Therefore, the two-photon resonance condition is satisfied through broad velocity groups.

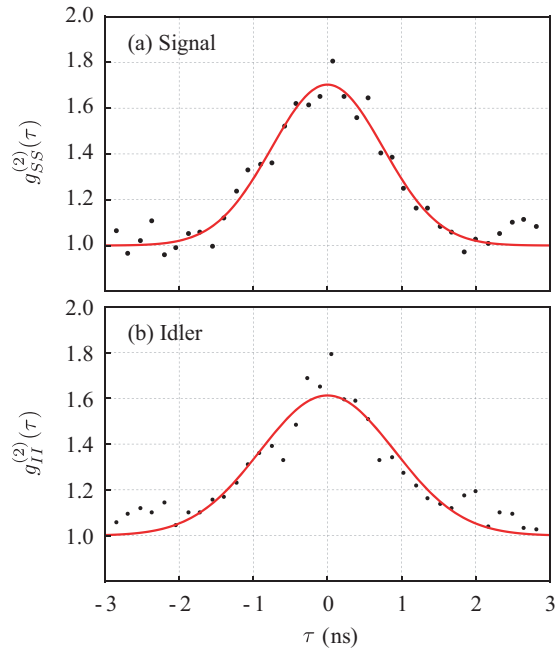


FIG. 3. Normalized autocorrelation functions for the signal and idler photons. The red solid curve is a Gaussian fitting to the experiment data. (a) The coherence time of the signal photons is estimated to be 1.8 ns. (b) The coherence time of the idler photons is estimated to be 2.1 ns.

III. NONLOCAL TWO-PHOTON INTERFERENCE

We measured the coherence time of each single photon to determine the path-length difference between the short path and the long path of the unbalanced Michelson-Morley interferometer (UMMI). We performed the Hanbury Brown–Twiss experiment by splitting the signal (idler) photons to two SPCMs by using the fiber beam splitter. Normalized autocorrelation functions for the signal and idler photons are shown in Fig. 3. The coherence times of the signal and idler photons are estimated to be 1.8 and 2.1 ns, respectively. To eliminate the first-order interference, we set the path-length difference between the long path and the short path of the UMMI to be 1.5 m, which is much longer than the coherence length of each single photon.

The experimental setup for nonlocal two-photon interference is shown in Fig. 1(c). The signal (idler) photons are divided into the two paths: The long path L_1 (L_2) and the short path S_1 (S_2), by the beam splitter (BS) in the UMMI. For the entangled photons traveling the long paths (L_1, L_2) or the short paths (S_1, S_2), the probability amplitudes for the entangled photons in the long and short paths are coherent. Then, interference between the probability amplitudes of both events occurs so that two-photon interference can be generated [33–35]. In contrast, if the entangled photons traverse the (L_1, S_2) or (S_1, L_2) path, interference between the probability amplitudes of both events cannot happen because of the path-length difference. Therefore, we post-select the coincidence events where two-photon interference occurs by the coincidence window of 5 ns.

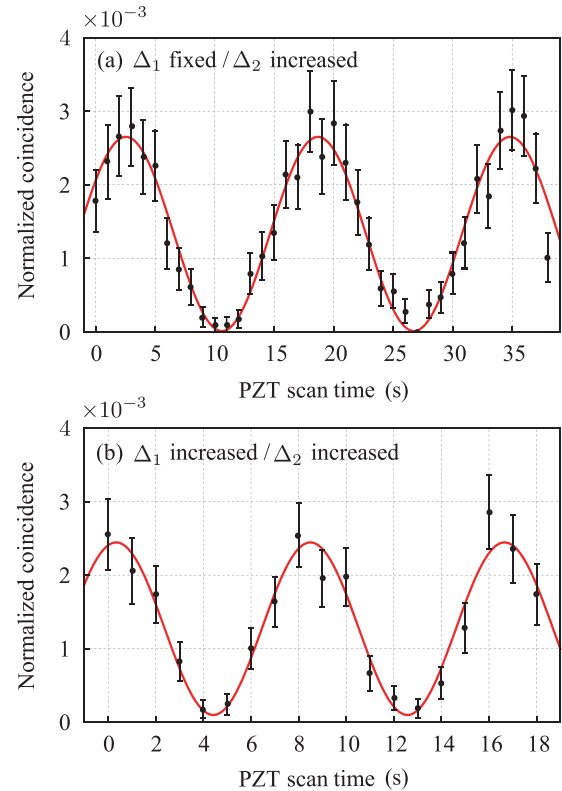


FIG. 4. Nonlocal two-photon interference; refer to Fig. 1(c). (a) The PZT2 is scanned with a constant speed, while the PZT1 is not. (b) The PZT1 and PZT2 are scanned in the same direction with the same speed as (a). Each data point is accumulated for 1 s. The red solid curve is a sinusoidal fitting for the experiment data. To accurately show the genuine second-order interference effect, the coincidence count rate N_c is normalized, i.e., $N_c/\sqrt{(N_s N_i)}$, where N_s and N_i are the single count rates for the signal and idler photons, respectively.

The entangled photon pair source and the interferometer are separated by a 180 m fiber; the travel time from the entangled photon pair source to the interferometer is 900 ns, which is much longer than the coincidence window, so both photons are separated at two spacelike locations. Therefore, two-photon interference is the nonlocal measurement outcome.

The coincidence rate exhibits a sinusoidal variation as a function of the path-length difference Δ_1 (Δ_2) controlled by the PZT. The coincidence rate of the two photons is then given by

$$P_{c.c.}(\Delta_1, \Delta_2) \propto \frac{1}{2} \left(1 + v \cos \left(\frac{\omega_S}{c} \Delta_1 + \frac{\omega_I}{c} \Delta_2 \right) \right), \quad (3)$$

where ω_S (ω_I) is the frequency of the signal (idler) photons and v is visibility. Only PZT2 is scanned in Fig. 4(a), but both PZTs are scanned in the same direction with the same speed as the previous one in Fig. 4(b). Therefore, in Fig. 4(a), the period of two-photon interference T_a is inversely proportional to ω_I . Similarly, in Fig. 4(b), the period of two-photon interference T_b is inversely proportional to summation of each single-photon's frequency $\omega_S + \omega_I$. In the experiment,

T_a/T_b was 1.96 ± 0.04 , which is similar to the ratio $(\omega_S + \omega_I)/\omega_I = 2.01$.

The visibility of two-photon interference in Fig. 4(a) is $97.1 \pm 2.5\%$, and that of two-photon interference in Fig. 4(b) is $90.5 \pm 4.0\%$. The minimum visibility of violation of the Bell-CHSH (Clauser-Horne-Shimony-Holt) inequality is 70.7% [36], so the Bell-CHSH inequality is violated by 10.5 and 4.9 standard deviations, as shown in Figs. 4(a) and 4(b), respectively.

IV. CONCLUSION

In conclusion, we have generated narrow-bandwidth energy-time entangled photon pairs via the SFWM process in warm ^{87}Rb vapor and experimentally shown nonlocal two-photon interference by using a Franson interferometer. For similar wavelengths of the pump and coupling beams counterpropagating the Doppler-broadened Rb ensemble, en-

tangled photon pairs which have a strong temporal correlation feature can be generated. The travel time of the single photons from the entangled photon pair source to the interferometer is much longer than the coincidence window, so two-photon interference satisfies the nonlocal condition. The visibility of two-photon interference is estimated to be $97.1 \pm 2.5\%$, so the Bell-CHSH inequality is violated by 10.5 standard deviations. We believe that the energy-time entangled photon pairs generated by the cascade emission in warm ^{87}Rb vapor via the SFWM process can be a source for long distance atom-memory-based quantum communication [37,38].

ACKNOWLEDGMENT

This work was supported by the National Research Foundation of Korea Grant No. 2019R1A2C3004812.

-
- [1] J. S. Bell, *Physics* **1**, 195 (1964).
 [2] O. Kwon, Y.-S. Ra, and Y.-H. Kim, *Opt. Express* **17**, 13059 (2009).
 [3] D.-G. Im, Y. Kim, and Y.-H. Kim, *Opt. Express* **27**, 7593 (2019).
 [4] D. F. Phillips, A. Fleischhauer, A. Mair, R. L. Walsworth, and M. D. Lukin, *Phys. Rev. Lett.* **86**, 783 (2001).
 [5] M. Fleischhauer and M. D. Lukin, *Phys. Rev. Lett.* **84**, 5094 (2000).
 [6] B. Julsgaard, J. Sherson, J. I. Cirac, J. Fiurášek, and E. S. Polzik, *Nature (London)* **432**, 482 (2004).
 [7] Y. Wang, J. Li, S. Zhang, K. Su, Y. Zhou, K. Liao, S. Du, H. Yan, and S.-L. Zhu, *Nat. Photonics* **13**, 346 (2019).
 [8] Y.-H. Chen, M.-J. Lee, I. Chung Wang, S. Du, Y.-F. Chen, Y.-C. Chen, and I. A. Yu, *Phys. Rev. Lett.* **110**, 083601 (2013).
 [9] M. Förtsch, J. U. Fürst, C. Wittmann, D. Strekalov, A. Aiello, M. V. Chekhova, C. Silberhorn, G. Leuchs, and C. Marquardt, *Nat. Commun.* **4**, 1818 (2013).
 [10] G. Schunk, U. Vogl, D. V. Strekalov, M. Förtsch, F. Sedlmeir, H. G. L. Schwefel, M. Göbelt, S. Christiansen, G. Leuchs, and C. Marquardt, *Optica* **2**, 773 (2015).
 [11] T.-M. Zhao, Y.-S. Ihn, and Y.-H. Kim, *Phys. Rev. Lett.* **122**, 123607 (2019).
 [12] A. Kuzmich, W. P. Bowen, A. D. Boozer, A. Boca, C. W. Chou, L.-M. Duan, and H. J. Kimble, *Nature (London)* **423**, 731 (2003).
 [13] L. Zhao, X. Guo, C. Liu, Y. Sun, M. M. T. Loy, and S. Du, *Optica* **1**, 84 (2014).
 [14] B. Srivathsan, G. K. Gulati, B. Chng, G. Maslennikov, D. Matsukevich, and C. Kurtsiefer, *Phys. Rev. Lett.* **111**, 123602 (2013).
 [15] C. Shu, P. Chen, T. K. A. Chow, L. Zhu, Y. Xiao, M. M. T. Loy, and S. Du, *Nat. Commun.* **7**, 12783 (2016).
 [16] D.-S. Ding, Z.-Y. Zhou, B.-S. Shi, X.-B. Zou, and G.-C. Guo, *Opt. Express* **10**, 11433 (2012).
 [17] Y.-S. Lee, S.-M. Lee, H. Kim, and H.-S. Moon, *Opt. Express* **24**, 28083 (2016).
 [18] P. G. Kwiat, A. M. Steinberg, and R. Y. Chiao, *Phys. Rev. A* **47**, R2472(R) (1993).
 [19] J. G. Rarity and P. R. Tapster, *Phys. Rev. A* **45**, 2052 (1992).
 [20] P. R. Tapster, J. G. Rarity, and P. C. M. Owens, *Phys. Rev. Lett.* **73**, 1923 (1994).
 [21] M. H. Rubin and Y. H. Shih, *Phys. Rev. A* **45**, 8138 (1992).
 [22] Y. H. Shih, A. V. Sergienko, and M. H. Rubin, *Phys. Rev. A* **47**, 1288 (1993).
 [23] D. V. Strekalov, T. B. Pittman, A. V. Sergienko, Y. H. Shih, and P. G. Kwiat, *Phys. Rev. A* **54**, R1(R) (1996).
 [24] P. G. Kwiat, W. A. Vareka, C. K. Hong, H. Nathel, and R. Y. Chiao, *Phys. Rev. A* **41**, 2910 (1990).
 [25] J. G. Rarity, P. R. Tapster, E. Jakeman, T. Larchuk, R. A. Campos, M. C. Teich, and B. E. A. Saleh, *Phys. Rev. Lett.* **65**, 1348 (1990).
 [26] J. D. Franson, *Phys. Rev. Lett.* **62**, 2205 (1989).
 [27] Y.-S. Ihn, Y. Kim, V. Tamma, and Y.-H. Kim, *Phys. Rev. Lett.* **119**, 263603 (2017).
 [28] O. Kwon, K.-K. Park, Y.-S. Ra, Y.-S. Kim, and Y.-H. Kim, *Opt. Express* **21**, 25492 (2013).
 [29] A. Martin, F. Kaiser, A. Vernier, A. Beveratos, V. Scarani, and S. Tanzilli, *Phys. Rev. A* **87**, 020301(R) (2013).
 [30] I. Marcikic, H. de Riedmatten, W. Tittel, H. Zbinden, M. Legré, and N. Gisin, *Phys. Rev. Lett.* **93**, 180502 (2004).
 [31] T. Honjo, S. W. Nam, H. Takesue, Q. Zhang, H. Kamada, Y. Nishida, O. Tadanaga, M. Asobe, B. Baek, R. Hadfield, S. Miki, M. Fujiwara, M. Sasaki, Z. Wang, K. Inoue, and Y. Yamamoto, *Opt. Express* **16**, 19118 (2008).
 [32] J. D. Franson, *Phys. Rev. A* **44**, 4552 (1991).
 [33] Y.-H. Kim and W. P. Grice, *J. Opt. Soc. Am. B* **22**, 493 (2005).
 [34] Y.-H. Kim, *J. Opt. Soc. Am. B* **20**, 1959 (2003).
 [35] Y.-H. Kim, V. Berardi, M. V. Chekhova, A. Garuccio, and Y. Shih, *Phys. Rev. A* **62**, 043820 (2000).
 [36] J. F. Clauser, M. A. Horne, A. Shimony, and R. A. Holt, *Phys. Rev. Lett.* **23**, 880 (1969).
 [37] T. Chanelière, D. N. Matsukevich, S. D. Jenkins, S.-Y. Lan, T. A. B. Kennedy, and A. Kuzmich, *Nature (London)* **438**, 833 (2005).
 [38] Y.-W. Cho and Y.-H. Kim, *Phys. Rev. A* **82**, 033830 (2010).